

Drive Chain Friction Characterization of a 6DOF Parallel Kinematics Robot

Hermes Giberti¹ ^a, Francesco La Mura¹ ^b, Ivan Raineri² and Marco Tarabini²

¹Università degli Studi di Pavia, Dipartimento di Ingegneria Industriale e dell'Informazione,
Via A. Ferrata 5, 27100 Pavia, Italy

²Politecnico di Milano, Department of Mechanical Engineering, Campus Bovisa Sud, via La Masa 1, 20156 Milano, Italy

Keywords: Ball-screw, Friction, PKM, Robot, Stribeck, Axis, Practical Approach, Stick Slip.

Abstract: This paper describes a time-efficient method for friction characterization on a Robot drive chain, namely a Ball-screw transmission. The Method promotes practical application by being independent from external sensors and giving very precise and usable output model. A complete estimation procedure is described together with the results obtained on the real Machine.

1 INTRODUCTION

This article describes the friction model identification methods used on the drive chain characterization of a 6DOF PKM. The case study of this work deal with the ball-screw drive o a parallel kinematics robot named *Hexafloat*, shown in fig.1.

An HIL (Hardware-In-the-Loop) architecture, requiring high dynamics, performances and safety, is deputed to simulate the ecosystem of an off-shore wind turbine. *Hexafloat* machine has to carry the scaled model of a floating wind turbine, and replicate the behaviour of its floating platform inside the wind gallery thanks to a complex real-time force control loop (Bayati et al., 2014; Bayati et al., 2017; Ferrari and Giberti, 2014; Fiore et al., 2016; Giberti and Ferrari, 2015; Giberti et al., 2018). For many safety and performance related reasons, a digital replication (Digital-Twin (Raineri et al., 2018)) of this robotic device as been created with the goal to preliminary test the architecture, develop control strategies (La Mura et al., 2018b; La Mura et al., 2018a) and check for control issues and performances lack (Silvestri et al., 2011; Confalonieri et al., 2018). In order to obtain Digital-Twin behaviour matches real device performances, accurate friction description is crucial.

Ball-screw direct coupling with Servo-Motor is an largely adopted solution in industrial field as well in robotics. Due to the optimal trade-off between precision and cost, they are often preferred to linear motors and belt transmissions given the lower energy ef-




Figure 1: The *Hexafloat*: a 6DOF PKM.


iciency of the former and the excessive deformability of the latter (Negahbani et al., 2016).

As empirical evidence witnessed, friction compensation is fundamental to improve the control performance of ball-screw mechanisms.

Olaru et Al. (Olaru et al., 2004) exploited roll contact theory with a modified Columbian model to provide an estimate of friction. Successive analysis carried out by Xu et Al. in (Xu et al., 2015) results in a creep friction model based on contact rheology which produces higher degree of accuracy for friction identification.

In real world applications however, system friction characterization often overlaps with system control. To this end, different strategies can be implemented and, to cope with increasing requirements of position accuracy, new and complex friction models have come to light. Frequency domain approaches

^a  <https://orcid.org/0000-0001-8840-8497>

^b  <https://orcid.org/0000-0001-5143-7120>

include the Differential Binary Squared Input as in (Chen et al., 2002) and the limit cycle analysis presented in (Kim and Chung, 2006). According to the time domain approaches, Lee et al. (Lee et al., 2015) proposed a PD feed drive position controller with observer-based friction compensator, Ro et al. (Ro et al., 2000) used a PD feed drive position controller with disturbance observer while Maeda and Iwasaki (Maeda and Iwasaki, 2013) developed an initial friction compensator. Keck et Al. (Keck et al., 2017) put forward an interesting identification methodology while applying feed-forward friction compensation based on Elasto-Plastic model. The aforementioned works address micro-positioning but, in many applications, the minimization of Steady-State error, although desirable, isn't a priority. If this is the case, the possibility to select a simpler, but yet physically meaningful, friction model whose parameters can be easily estimated is enticing. This holds especially true when ball-screw characterization is an aspect of a wider picture.

This paper aims at proposing a new, practical method to characterize friction in ball-screw actuators, developing and refining previous ideas found in literature (Keck et al., 2017). The method will be independent from external sensors while having an optimized test total time and cost. Thanks to a suited experimental campaign, a peculiar friction induced phenomenon has been observed and estimated. The influences of the so called Stick-Slip effect on the overall friction behaviour led to the selection of three friction models with increasing complexity; with the objective to describe comprehensively the overall frictional trend. Parameters identification is performed for each model while pro and cons are highlighted.

2 SYSTEM MODELING

The robot is made of 6 identical kinematic chains, each of which composed by two passive universal joints, a link with free axial rotation, a carriage holding one of the universal joints and a drive chain. Each drive chain is made by three main components as depicted in Fig 2: a) A brushless motor, that provides the torque; b) A torsionally rigid coupling, that transmits torque from the motor shaft to the ball-screw; c) Ball-Screw, it transforms rotary motion into linear motion and carries the load attached to the nut. It's the main responsible for friction losses.

Admitting the hypothesis of rigid bodies, it is possible to transform the system in an equivalent SDOF translating system. The second order differential dy-

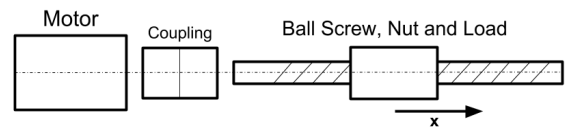


Figure 2: Main components of a ball-screw actuator.

amic equation ruling the system is:

$$M_{equivalent} \ddot{x} = F_{motor} - F_{friction}(v) - F_{load} \quad (1)$$

Being $F_{motor} = \frac{C_{motor}}{\tau}$ with τ the transmission rate. In the case of ball-screw $\tau = [\frac{m}{rad}] = \frac{lead}{2\pi}$. Let's now impose a zero load condition $F_{load} = 0$ for the sake of identification by disconnecting the transmission from the other robot components. Additionally, the equation at equilibrium $\ddot{x} = 0$, offers a useful representation as in Eq 1:

$$0 = F_{motor} - F_{friction}(v) \Rightarrow F_{motor} = F_{friction}(v) \quad (2)$$

It is thus possible to use a constant velocity motion law to exploit Eq 2 and map the $F_{friction}$ through F_{motor} . A displacement motion law, created appending various ramps with different slopes, can test friction force for velocities corresponding to the slope of each ramp.

3 PROPOSED METHOD

The proposed method articulates in four phases: 1) creation of a suitable test motion law; 2) execution of the aforementioned motion law and collection of servo-motor torque signal; 3) data-set batch processing; 4) Identification of parameters for the different friction Models. The main idea behind this procedure is to feed the controller with a reference displacement made up of ramps and rests, collect the servo-motor torque readings and obtain the mean value of motor action for each tested velocity.

3.1 Friction Models

Among many different possibilities, pursuing a proper balance between model complexity and completeness, three friction models are selected: Stribeck model, modified Stribeck model and Neural Network (NN) model.

Stribeck: In presence of lubrication, friction force can be described with Stribeck Model as in Fig 3

It features a smooth and continuous transition from the static region to the dynamic region. This model is completely described by a set of 9 parameters: $[F_s^+, F_c^+, F_v^+, v_s^+, F_s^-, F_c^-, F_v^-, v_s^-, \delta]$. They are respectively: F_s^+ is the Static friction force (this represents

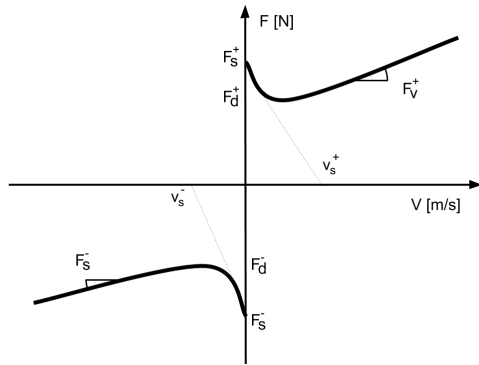


Figure 3: Stribeck friction.

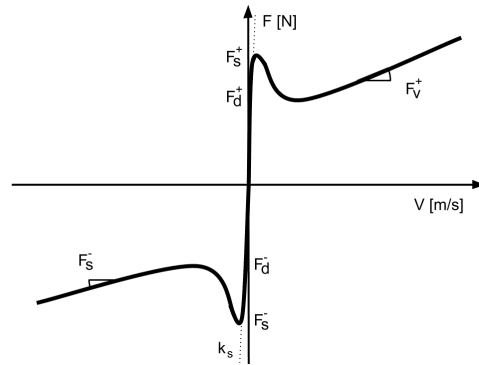


Figure 4: Modified Stribeck friction.

the maximum force opposing the motion when system is at rest), F_c is the Columbian friction force (the minimum force opposing the motion when system is moving), F_v is the Viscous component of the friction force (it is proportional to the velocity), v_s is the Stribeck velocity (this is the parameter ruling the exponential envelope of Stribeck curve) and δ is the additional parameter which shapes the exponential envelope.

Each of the parameters, except δ , takes different values depending on the sign of velocity so that a total number of nine parameters is reached. Extending the Armstrong-Hélouvy formulation for negative and positive signs, the analytical expression of Stribeck effect is:

$$\begin{cases} F_f = F_c^+ + (F_s^+ - F_c^+)e^{-(v/v_s^+)^\delta} + F_v^+ v & \text{for } v > 0 \\ F_f = F_c^- + (F_s^- - F_c^-)e^{-(v/v_s^-)^\delta} + F_v^- v & \text{for } v < 0 \end{cases}$$

Having considered the wide variability of the delta value throughout literature and the lack of general rules to assume its value a priori, it was chosen to include it in the parameter estimation for the sake of completeness.

Modified Stribeck: Although theorized to enhance simulation capabilities (Andersson et al., 2007), this model features an additional parameter which rules the envelope of a $\tan(h)$ function. The analytic description is:

$$\begin{cases} F_f = F_c^+ + (F_s^+ - F_c^+)e^{-(v/v_s^+)^\delta} \tan(k_s v) + F_v^+ v & \text{for } v > 0 \\ F_f = F_c^- + (F_s^- - F_c^-)e^{-(v/v_s^-)^\delta} \tan(k_s v) + F_v^- v & \text{for } v < 0 \end{cases}$$

As can be seen in Fig 4, the curve corresponds to the Stribeck model excepts in the x neighbourhood of the origin, where it tends to zero. This interval widens as k_s approaches to zero.

Neural Network: Neural Networks identification offers a model through implicit variables. This approach is interesting to identification needs since it can pick

up unmodeled peculiarities of the motor-ballscrew system. Among them: directional anisotropy of the ball-screw transmission, coupled vibration-friction phenomena and non-Newtonian behaviour of lubricant. On the other hand, the estimated parameters could have no direct physical interpretation. However, assuming friction force $F_{friction}(v)$ is a function of velocity only, the diagram can be simplified. A compact notation expressing the relationship between input and output takes this shape:

$$\underline{u} = \sigma(\underline{w}v + \underline{b}); \quad F_{friction} = \sigma(\underline{w}'^T \underline{u} + b') \quad (3)$$

where w and w' are the weights vectors and represents connection importance between two neurons of different layers, \underline{u}_j is the activation state vector for hidden layer neurons, b and b' are the bias vectors concurring at activation state determination and σ is the squashing or activation function.

3.2 Stick-Slip

The friction-induced Stick-Slip effect consists in a jerky alternation of rest and motion phases. This phenomenon manifests at low velocities with a cyclic transition from dynamic to static condition and the other way around. The presence of Stick-Slip may modify macroscopically the friction nature approaching the zero velocity region.

3.3 Test Motion Law

The first step to take in this phase is to select a set of absolute values of velocities to test. In this effort, it is advisable to generate the set by using a polynomial of the type:

$$v_i = a_0 + \sum_{j=1}^J a_j i^j \quad (4)$$

where v_i is the i^{th} element of the set and J is the order of the polynomial. By opportunely choosing the degree of the polynomial and the linear coefficients a_j ,

it is possible to distribute the test velocities expediently. In general, it is preferable to test a bigger number of lower magnitude velocities, corresponding to static-dynamic transition region, while consider less high-magnitude velocities attaining the viscous effect region characterized by a more constant slope. In a second instance, an observation reference $x = 0$ is selected, this position is preferably the midpoint of the axis to avoid other phenomena affecting extreme axis position and enhance travelling distances. Concurrently, an observation band is placed about the reference position. This band is suitable for discarding acceleration and deceleration transient phases from acquisition.

Right after, a motion law consisting of an alternation of ramps and rest phases has to be generated. The slope of the ramps is imposed by the velocities set determined at the previous step. For each step, both negative and positive sign should be considered consequentially as suggested in (Keck et al., 2017).

Please notice that, as the magnitude of tested velocity increases, the slider should travel further from the observation band in order to guarantee that the controller is able to enforce constant velocity during the observation band cross-over. Position extremes to be touched by the motion law in dependence from velocity, as described by the following equation:

$$\begin{cases} x_{i+} = +q + m v & \text{for } v > 0 \\ x_{i-} = -q + m_i v & \text{for } v < 0 \end{cases}$$

where, at least, $q_i > \frac{\delta x_i}{2}$. In order to guarantee smoother transients, the ramp can be modified in a symmetrical trapezoidal velocity profile. Aggressive controls with relevant feed-forward contributions especially benefit from this practice. To implement such a strategy, let's consider the travel distance

$$q_f = x_{extreme}^{k+1} - x_{extreme}^k$$

the velocity to test V and the maximum acceleration at disposal a . Trough the well known formulas of trapezoidal motion law, shown in Fig 5, it is possible to build the motion law and estimate the total time T needed to perform the smoothed ramp. After each ramp, a rest phase of $1s$, is observed to minimize the influence of possible vibrations occurring in lower stiffness systems at the end of the motion.

The sequence of ramps, with alternate slope sign, and rests results in a motion law that hovers around the observation reference, if initial condition $x_{extreme}^0 = \pm \frac{q}{2}$ is assumed. It is now possible to consider the sum of ramps and rests times composing the motion law total time T_{total} :

$$T_{total} = T_{total}(N, [a_0, a_1, \dots, a_J], q, m, \delta x) \quad (5)$$

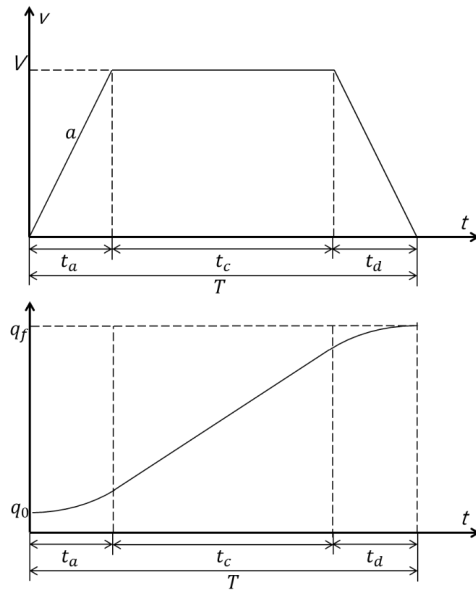


Figure 5: Trapezoidal Motion Law.

As a function of the number of velocities N to test, the coefficients of the polynomial a_j , the couple (q, m) and the observation band δx . While this function is sensitive to each of these inputs, it is especially effective to adopt a multi-band approach with the aim to minimize the total execution time T_{total} . By considering narrower observation bands on the lower velocity ramps, it is possible to significantly reduce T_{total} while maintaining wider bands for the faster ones in order to represent them properly. In general, it is possible to state that:

$$T_{total} = (N, [a_0, a_1, \dots, a_J], q, m, [\delta x_1, \delta x_2, \dots, \delta x_K], g(i)) \quad (6)$$

where $[\delta x_1, \delta x_2, \dots, \delta x_K]$ are the K bands and $g(i)$ is a function of the i^{th} tested velocity ruling when a band succeeds to another. By tuning those parameters it is possible to save significant execution time.

Once the motion law is executed, it is useful to verify that the controller is actually capable to cope with the requirements so that actual velocity is almost identical to the reference one. If this requirement is satisfied, then the Servo-Motor data collected during motion law execution can be trusted. Motor action time history is sliced in buffers with different ramp lengths. For each segment attaining to the single ramp, only the section related to observation band cross-over is considered. Mean is taken over those intervals resulting in the motor average action for each tested velocity across its proper observation band. Those data constitute the foundation for identification. The velocity-force pairs can be plotted on a graphic to provide visual feedback representation.

3.4 Identification of Friction Model Parameters

The final step of the proposed method consists in identification of parameters. To this purpose, a LSQ – Least Square – identification is put forward. The mean residual square error e_{RMS} can be considered as a figure of merit of the identification. If the test velocities selection has been carried out wisely, there should be no need to introduce weights. To solve the minimization problem, a genetic algorithm is deployed since its low dependency from initial guess.

Depending on the tested velocity and on the peculiarities of the system object of identification, it is possible Stick-Slip effects acquisitions under certain velocity limit. Anyhow, those influences smooth out as velocity increases. When the vibration produced by Stick-Slip is not negligible for some of the tested velocities, actions should be taken accordingly to the friction models chosen for identification. To improve *Stribeck model* parameter estimation, it is better to purge experimental data from Stick-Slip affected samples, while *Modified Stribeck model* and *NN model* can better pick up this peculiarity.

4 EXPERIMENTAL SETUP

As said in Section 2 and going into further technical details, the drive chain of *Hexafloat* is made of a TH145 SP4 ball screw linear axis by Rollon, a Toolflex 20M coupling and a RM88-K2K030C-BS2 servo motor by Omron.

The servo motor is provided with a 20bit high-resolution incremental encoder that provides position feedback to the controller with an accuracy of $131072 \frac{cnt}{rev} = 3277 \frac{cnt}{mm}$. In the mean time, the controller keeps a data log of the computed action during motion execution.

To the purpose of this experiment, robot leg is dismounted from the slider to eliminate F_{load} from eq.1. This process is also unavoidable, since the parallel nature of the robot, to safely move one slider at a time with large displacements. Fig. 6 shows the leg disassembled from the slider.

For the Stick-Slip phenomenon, a dedicated experiment has been setup, using an external laser sensor to measure local vibration of the slider when subject to low motor driving torques. During this experiment, the sensor is positioned so that the slider can move in a range of 4 mm without getting out of focus. The measurement scheme is reported in fig 7.

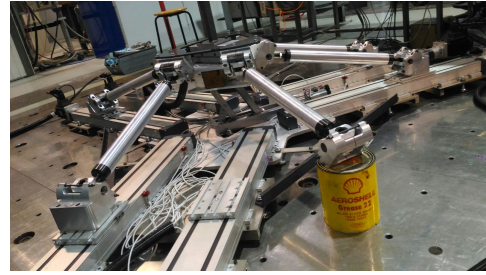


Figure 6: Experimental Set-Up.

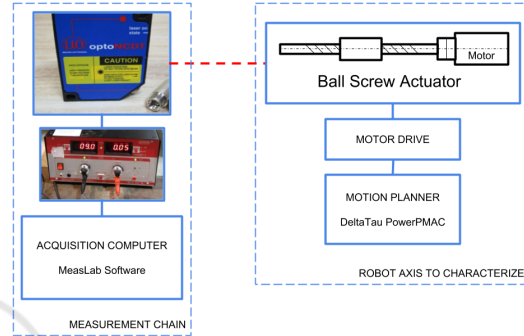


Figure 7: Experimental setup for Stick-Slip inquiry.

5 EXPERIMENTAL RESULTS

In this section the proposed method is applied. A 3th degree polynomial is used to generate the test set with the coefficients hereafter summarized: $a_0 = 100 \times 10^{-7}$, $a_1 = 100 \times 10^{-7}$, $a_2 = 40 \times 10^{-7}$, $a_3 = 3 \times 10^{-7}$.

A total of $N = 51$ velocities exploring the interval $(0.02 - 50) \times 10^{-3} \frac{m}{s}$. Following the prescriptions reported in 3.3, a first attempt motion law is designed with an observation band $\delta x = 10 \text{ mm}$. The generated motion law is excessively time consuming in the first ramps. In order to minimize the total motion law execution time T_{total} , a three band approach is adopted. The observation band value for each ramp is described by: $\delta x_1 = 2 \text{ mm}$ for first three velocities, $\delta x_2 = 5 \text{ mm}$ for the fourth, fifth and sixth velocity and $\delta x_3 = 10 \text{ mm}$ for all the others.

The optimized motion law saves a considerable time and results in a $T_{total}^{multi\ band} < \frac{1}{3} T_{total}^{one\ band}$. Fig 8 provides the graphical representation of multi-band approach motion law.

Motion law is implemented inside robot motion controller, for the axis object of the characterization. During motion execution, the data log of control action is registered as well as the actual position i.e. internal encoder measurements. The results on the latter show that the controller can actually follow the reference as expected. The former is stored and keep

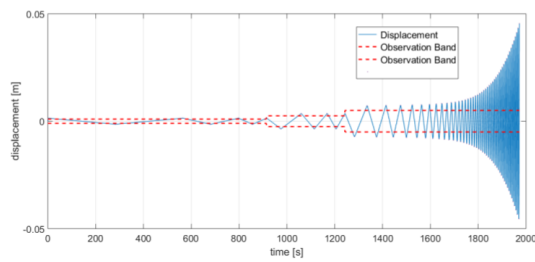


Figure 8: 1 Band vs 3 Bands approach, time comparison.

for further processing. Fig 9 displays the Reference Motor Action time history. As can be noticed, when the velocity changes from positive (upward ramp) via zero (rest phase) to negative (downward ramp) and vice-versa, the control effort undergoes to significant variations. Conversely, during ramp motion, the change is considerably reduced.

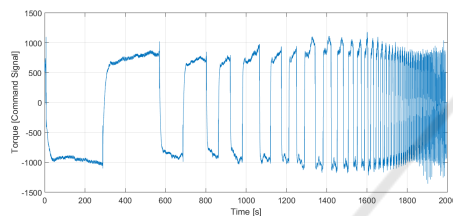


Figure 9: Reference Motor Action.

After applying the averaging process described in the 3.3, the velocity-force pairs are plotted in Fig 10.

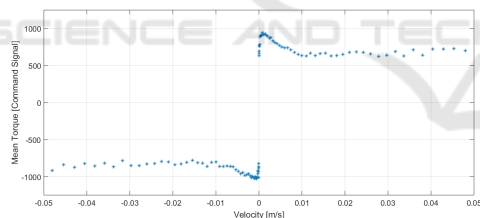


Figure 10: Experimental Results. Velocity-MeanMotorTorque pairs.

In a glance, it is possible to observe a general analogy with Stribeck curve. On the other hand, the points related to low velocity ramps appear not to fit into the normal *Stribeck* framework presented in 3.1. In particular, friction caused torque seems to lessen with respect to "static" equivalent value for a very narrow velocity band around zero value. The next section explores this behaviour with insights on the stick-slip phenomenon.

5.1 Stick-Slip Influence

As previously stated, Stick-Slip is a friction-induced phenomenon occurring at low velocities. It consists in a continuous transition from motion (slip phase)

to rest (stick phase) and vice-versa (Berman et al., 1996). In order to better understand the influence of this phenomenon on the axis dynamics, stick-slip inquiries are executed. For the sake of brevity and considering the supportive-only nature of this experiment with respect to the method, we won't dig into details. Several tests are done and the motor is driven at different constant velocities. A triangulation laser measures the local displacement perturbations of the slider, resulting from stick-slip induced vibrations. Fig. 11 shows an example of the phenomenon measured, fig. 12 reports the experimental campaign and fig. 13 a detail of the previous, particularly important for the discussion.

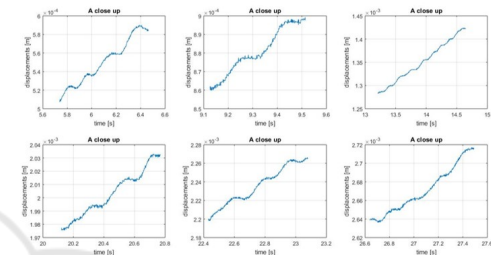


Figure 11: Measured Stick-Slip phenomenon.

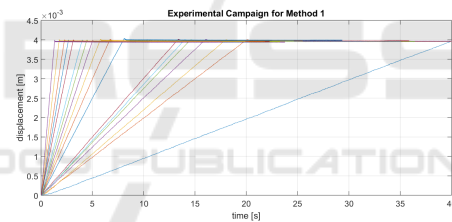


Figure 12: Stick-Slip Experiments.

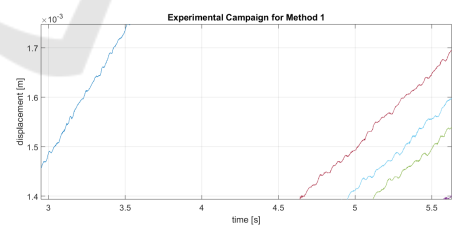


Figure 13: A Particular.

Analysing fig. 13, it is possible to notice a group of three tests on the right and compare it to the one on the left. As observed in the driving velocities range of $(0.5 - 0.3) \times 10^{-3} m/s$, the influence of vibratory phenomenon gradually smooths out. In this region is no longer possible to clearly identify rest-slip phases like in fig. 11. Although identification of a precise Stick-Slip critical transient velocity has not been possible, it seems reasonable enough to consider this speed within this band. For the sake of clarity from now on this interval will be called *Experimental Vi-*

bration Smoothing Interval. Switching back to the preliminary result obtained in the previous section, the following relation exists: all the points not fitting the Stribeck model are related to ramps whose velocity is below the Vibration Smoothing Interval, while for other acquisitions, no clear evidences of Stick-Slip occurrence have been found.

Thus one can assume that microscopic vibration induced by Stick-Slip reduces the macroscopic friction force. This hypothesis can be supported by two different standpoint: a) A comparison can be drawn with the control technique called high frequency dithering; b) the microscopic entanglements between surfaces do not bound effectively when disturbed by a local vibration of the interfaces. To confirm this hypothesis further research are required.

Eliminating the data affected by Stick-Slip phenomenon, one can refine the test results in the one depicted in Fig 14. Parameter estimation is performed on those data.

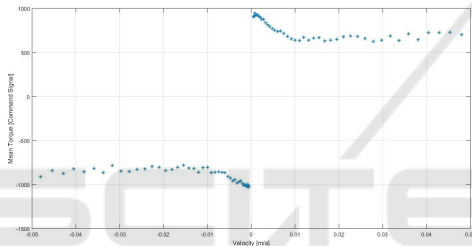


Figure 14: Refined Test Result.

6 MODEL PARAMETERS IDENTIFICATION

Parameter identification is carried out according to the methodology exposed in section 3. The genetic algorithm runs with an initial population of 10.000 individuals, maximum generation equal to 100 and a mutation rate of 0.8. Additionally, the initial population algorithm is endowed with a custom initial population based on Divide-and-Conquer paradigm to enhance convergence efficiency. Results are satisfactory as can be seen in Fig 15. Tab 1 reports the numerical values for completeness sake.

Table 1: Identified Stribeck friction Parameters.

F_s^+	F_c^+	v_s^+	δ	F_s^-
944.2	6111.8	0.0065	1.26	1049.2
F_c^-	v_s^-	F_v^+	F_v^-	e_{RMS}
750.9	0.0074	1904.2	2565.0	11.4

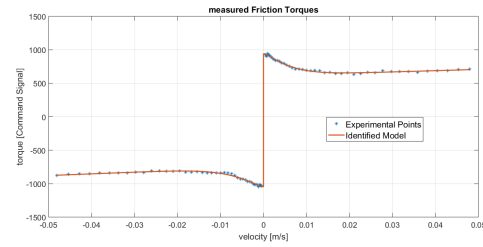


Figure 15: Identified Model.

7 CONCLUSIONS

In this article a simple and efficient friction estimation methodology is proposed for the drive chain of a PKM.

The proposed procedure successfully use servo motor torque estimation and velocity measurements to create velocity-force mapping, without the usage of additional sensors and acquisition system over the machine itself and its servo driver. The Stick-Slip phenomenon has been also analyzed, together with its influence on acquired data and methods for extracting a good model despite its effects. The model parameters have been computed fitting experimental data with a custom genetic algorithm and solving an LSQ problem. The results show a satisfactory match between model and real data. This model is implemented inside the Digital Twin of the *Hexafloat* robot. Given the exact same tool centre point position time history as reference and the exact same control architecture and gains, the command torque of the motors acquired in both real and simulated case are shown in fig.16. Results match satisfactory, even considering flexible dynamics and other source of approximation inside the digital replication of the machine that may lead to very different actuators efforts.

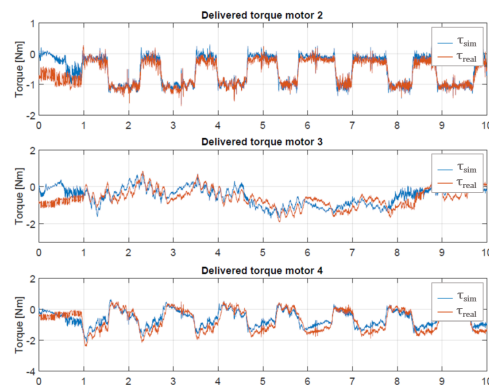


Figure 16: Digital Twin command torque comparison with real control effort.

REFERENCES

- Andersson, S., Söderberg, A., and Björklund, S. (2007). Friction models for sliding dry, boundary and mixed lubricated contacts. *Tribology international*, 40(4):580–587.
- Bayati, I., Belloli, M., Bernini, L., Giberti, H., and Zasso, A. (2017). Scale model technology for floating offshore wind turbines. *IET Renewable Power Generation*, 11(9):1120–1126.
- Bayati, I., Belloli, M., Ferrari, D., Fossati, F., and Giberti, H. (2014). Design of a 6-dof robotic platform for wind tunnel tests of floating wind turbines. *Energy Procedia*, 53:313–323.
- Berman, A., Ducker, W., and Israelachvili, J. (1996). Origin and characterization of different stick-slip friction mechanisms. *Langmuir*, 12(19).
- Chen, Y.-Y., Huang, P.-Y., and Yen, J.-Y. (2002). Frequency-domain identification algorithms for servo systems with friction. *IEEE transactions on control systems technology*, 10(5):654–665.
- Confalonieri, M., Ferrario, A., and Silvestri, M. (2018). Calibration of an on-board positioning correction system for micro-edm machines. In *EUSPEN Conference Proceedings - 18th International Conference and Exhibition*, pages 153–154.
- Ferrari, D. and Giberti, H. (2014). A genetic algorithm approach to the kinematic synthesis of a 6-dof parallel manipulator. In *2014 IEEE Conference on Control Applications (CCA)*, pages 222–227.
- Fiore, E., Giberti, H., and Ferrari, D. (2016). Dynamics modeling and accuracy evaluation of a 6-dof hexaslide robot. In *Nonlinear Dynamics, Volume 1*, pages 473–479. Springer.
- Giberti, H. and Ferrari, D. (2015). A novel hardware-in-the-loop device for floating offshore wind turbines and sailing boats. *Mechanism and Machine Theory*, 85(Supplement C):82 – 105.
- Giberti, H., La Mura, F., Resmini, G., and Parmeggiani, M. (2018). Fully mechatronical design of an hil system for floating devices. *Robotics*, 7(3):39.
- Keck, A., Zimmermann, J., and Sawodny, O. (2017). Friction parameter identification and compensation using the elastoplastic friction model. *Mechatronics*, 47:168–182.
- Kim, M.-S. and Chung, S.-C. (2006). Friction identification of ball-screw driven servomechanisms through the limit cycle analysis. *Mechatronics*, 16(2):131–140.
- La Mura, F., Romanó, P., Fiore, E., and Giberti, H. (2018a). Workspace limiting strategy for 6 dof force controlled pkms manipulating high inertia objects. *Robotics*, 7(1):10.
- La Mura, F., Todeschini, G., and Giberti, H. (2018b). High performance motion-planner architecture for hardware-in-the-loop system based on position-based-admittance-control. *Robotics*, 7(1):8.
- Lee, W., Lee, C.-Y., Jeong, Y. H., and Min, B.-K. (2015). Distributed component friction model for precision control of a feed drive system. *IEEE/ASME Transactions on Mechatronics*, 20(4):1966–1974.
- Maeda, Y. and Iwasaki, M. (2013). Initial friction compensation using rheology-based rolling friction model in fast and precise positioning. *IEEE Transactions on Industrial Electronics*, 60(9):3865–3876.
- Negahbani, N., Giberti, H., and Fiore, E. (2016). Error analysis and adaptive-robust control of a 6-dof parallel robot with ball-screw drive actuators. *Journal of Robotics*, 2016.
- Olaru, D., Puiu, G. C., Balan, L. C., and Puiu, V. (2004). A new model to estimate friction torque in a ball screw system. In *Product engineering*, pages 333–346. Springer.
- Raineri, I., La Mura, F., and Giberti, H. (2018). Digital twin development of hexafloat, a 6dof pkm for hil tests. In *The International Conference of IFToMM ITALY*, pages 258–266. Springer.
- Ro, P. I., Shim, W., and Jeong, S. (2000). Robust friction compensation for submicrometer positioning and tracking for a ball-screw-driven slide system. *Precision Engineering*, 24(2):160–173.
- Silvestri, M., Pedrazzoli, P., Boër, C., and Rovere, D. (2011). Compensating high precision positioning machine tools by a self learning capable controller. In *Proceedings of the 11th international conference of the european society for precision engineering and nanotechnology*, pages 121–124.
- Xu, N., Tang, W., Chen, Y., Bao, D., and Guo, Y. (2015). Modeling analysis and experimental study for the friction of a ball screw. *Mechanism and Machine Theory*, 87:57–69.